Ocean Modelling 28 (2009) 106–117

Contents lists available at ScienceDirect

Ocean Modelling

journal homepage: www.elsevier.com/locate/ocemod

Comparison of unstructured, staggered grid methods for the shallow water equations

R.A. Walters [a,*], Emmanuel Hanert [b], J. Pietrzak [c], D.Y. Le Roux [d]

[a] Hydrodynamics, O/RM, 6051 Hunt Rd, Victoria, Canada BC V8Y 3H7
[b] Department of Environmental Sciences and Land Use Planning, Université catholique de Louvain, Croix du Sud 2/16, B-1348 Louvain-la-Neuve, Belgium
[c] Faculteit CiTG, TU Delft, Stevinweg 1, 2628 CN Delft, The Netherlands
[d] Institut Camille Jordan, Université Claude Bernard Lyon 1, 43 Boulevard du 11 novembre 1918, 69622 Villeurbanne cedex, France

ARTICLE INFO

Article history:
Received 3 May 2008
Received in revised form 10 November 2008
Accepted 11 December 2008
Available online 27 December 2008

Keywords:
Shallow water equations
Unstructured grid
Finite element
Finite difference
Finite volume

ABSTRACT

Unstructured grid models are receiving increased attention mainly because of their ability to provide a flexible spatial discretization. Hence, some areas can be resolved in great detail while not over-resolving other areas. Development of these models is an ongoing process with significant longstanding issues with spurious computational modes, efficiency, advection and Coriolis approximations, and so forth. However, many of these problems have been solved with the current generation of models which have much promise for coastal to global scale ocean modelling. Our purpose is to intercompare a class of unstructured grid models where the continuity equation reduces to a finite volume approximation. The momentum equations can be approximated with finite difference, finite element, or finite volume methods. Each of these methods can have advantages and disadvantages in different classes of problems that range from hydraulics to coastal and global ocean flows. Some of the more important differences are restrictions on grid irregularity and stability of the Coriolis term. The finite element version of the model has important advantages in the discretization of the Coriolis term and does not require a reconstruction of a tangential velocity component. The comparison is illustrated with a simple test case.

1. Introduction

The shallow water equations (SWE) have wide application in oceanography, hydraulics, and atmospheric sciences. They contain the essential dynamics for most geophysical flows and form the focus for this study. As may be expected, there is a wide range of numerical methods useful for solving these equations, including finite difference (FD), finite element (FE), and finite volume (FV) methods.

Early in the application of numerical methods to the SWE, spurious computational modes were observed in methods that used the primitive equations and located dependent variables for sea level and velocity at the same nodes. This problem is now well understood (Walters and Carey, 1983; Le Roux et al., 2007) and many if not most models use some form of a staggered grid where sea level and velocity are discretized differently.

For oceanic flows, the important wave dynamics includes gravity waves and the effect of the Coriolis force. Hence these models must accurately reproduce simple gravity waves, Kelvin waves, Poincaré waves, and Rossby waves. Many of these models use structured, staggered FD grids (Griffies et al., 2000). More recent models use unstructured grids and a variety of FD (Casulli and Walters, 2000; Fringer et al., 2006; Casulli and Zanolli, 2002), FE (Walters and Casulli, 1998; Le Roux et al., 2000; Danilov et al., 2004; Pain et al., 2005; Hanert et al., 2005; White et al., 2008; Lane et al., 2009), and FV methods (Bradford and Sanders, 2002; Chen et al., 2003).

For hydraulics problems, the important dynamics includes gravity flows with relatively large Froude number (Fr) and transcritical flows. The corresponding numerical models must treat advection and shocks accurately. Hence the models generally use the conservative form of the momentum equation with energy or momentum conserving discretizations for advection (Stelling and Duinmeijer, 2003) or with Riemann methods (Toro, 1997; Denlinger and Iverson, 2001). Note that these same considerations also apply to ocean models when tsunami runup with high Fr is included.

Research over the last decade has led to a convergence of several solution methods that use unstructured grids. These methods use a finite volume form of the continuity equation and then discretize the momentum equation with either FD (Casulli and Walters, 2000; Casulli and Zanolli, 2002; Fringer et al., 2006), FE (Walters and Casulli, 1998; Miglio et al., 1999), or FV (Bradford

* Corresponding author. Tel.: +1 250 652 8995.
E-mail addresses: rawalters@shaw.ca (R.A. Walters), emmanuel.hanert@uclouvain.be (E. Hanert), J.D.Pietrzak@tudelft.nl (J. Pietrzak), dleroux@math.univ-lyon1.fr (D.Y. Le Roux).

1463-5003/$ - see front matter © 2008 Elsevier Ltd. All rights reserved.
doi:10.1016/j.ocemod.2008.12.004

and Sanders, 2002) methods. Hence the discretization of the momentum equation defines the specific method that is used. Two of these approaches are attractive for ocean models – one uses a FE approach with the RT_0 element (Raviart and Thomas, 1977; Walters and Casulli, 1998), and the other uses a FD approach on an unstructured grid (Casulli and Walters, 2000). Both of these approaches require a careful treatment of the Coriolis term both spatially and temporally.

In general, the FV modeling approach uses depth and flux as the dependent variables. The use of depth is appealing for hydraulic problems but presents difficulties for ocean models. The horizontal pressure gradient force depends on sea level gradient rather than depth gradient. Hence the forcing term is split into a depth gradient and a bottom gradient which are of the same order. This gives rise to a source balancing problem inherent in many FV models. In addition, the ratio of sea level elevation and water depth is large which leads to further problems with truncation errors. As a result, we will not consider the FV approach further since our interest is in ocean models.

Our purpose in this study is to compare and contrast the approximations and constraints inherent in certain unstructured, staggered grid FE and FD methods. Here, we define unstructured staggered grids to mean those discretizations that have one degree of freedom for the normal component of velocity on each element edge and one degree of freedom for sea level on each element. For structured FD grids, this is just the C-grid. While the various unstructured staggered grid approaches have similarities, there are also many differences in the approximations of the individual terms. These lead to constraints that may affect stability, accuracy, and/or efficiency.

In the next section, we define the governing equations and the numerical approximations with particular attention to the differences in the formulations. Next is a section that discusses the discretization of the Coriolis term. The section following includes some discussion of the properties of the methods. Finally, we present a simple numerical example and conclusions.

2. Formulation

2.1. Shallow water equations

The basic equations considered here are the three-dimensional shallow water equations. These equations are derived from the Reynolds-averaged Navier–Stokes equations by using the hydrostatic assumption and the Boussinesq approximation. For incompressible flows the continuity equation (incompressibility constraint) is

$$\nabla \cdot \mathbf{u} + \frac{\partial w}{\partial z} = 0 \tag{1}$$

and the momentum equation expressed in non-conservative form is

$$\frac{D\mathbf{u}}{Dt} + f\hat{\mathbf{z}} \times \mathbf{u} + g\nabla\eta - \frac{\partial}{\partial z}\left(A_v \frac{\partial \mathbf{u}}{\partial z}\right) - \nabla \cdot (A_h \nabla \mathbf{u}) = 0 \tag{2}$$

where the coordinate directions (x,y,z) are aligned in the east, north, and vertical directions; $\mathbf{u}\ (x,y,z,t)$ is the horizontal velocity with components (u,v); $w(x,y,z,t)$ is the vertical velocity; f is the Coriolis parameter; $\hat{\mathbf{z}}$ is the upward unit vector; $\eta(x,y,t)$ is the distance from the reference elevation to the free surface; g is the gravitational acceleration; A_v and A_h are the kinematic vertical and horizontal viscosities, respectively; and ∇ is the horizontal gradient operator $(\partial/\partial x, \partial/\partial y)$.

The two-dimensional vertically-averaged form of (2) is similar with $\mathbf{u}$ replaced by the depth-averaged value and the vertical stress term replaced by $(\tau_s - \tau_b)/\rho H$ where τ_b is the bottom stress and τ_s is the surface stress which is neglected here. For instance, see the development in Pinder and Gray (1977) or many other publications.

The bottom stress τ_b is given by

$$\frac{\tau_b}{\rho} = C_D|\mathbf{u}|\mathbf{u} = \gamma\mathbf{u} \quad (z = h), \tag{3}$$

where ρ is a reference density, C_D is a bottom drag coefficient, $h(x,y)$ is the bottom elevation measured from a reference elevation such that $H(x,y,t)$ is the total water depth given by $H = \eta - h$, and γ is defined by this equation.

The free surface equation is derived by vertically-integrating the continuity equation and using the kinematic free surface and bottom boundary conditions (Pinder and Gray, 1977).

$$\frac{\partial \eta}{\partial t} + \nabla \cdot \left(\int_h^\eta \mathbf{u} dz\right) = 0 \tag{4}$$

Boundary conditions for (1)–(4) generally fall into two categories: conditions at open (sea) boundaries and conditions at solid (land) boundaries. At open boundaries sea level η, radiation conditions, or a combination of these are generally set. In addition, discharge may be specified for river or other inflow. At land boundaries, the normal component of velocity vanishes so that $(\mathbf{u} \cdot \hat{\mathbf{n}}) = 0$ where $\hat{\mathbf{n}}$ is the unit normal. If the flow is viscous, then stress conditions also need to be specifed. Either a stress condition is specified by (3) or $\mathbf{u}|_h = 0$ and the bottom boundary layer needs to be resolved by the vertical grid placement.

2.2. Time discretization

The equations are discretized in time using a semi-implicit method such that the equations are evaluated in the time interval $\Delta t = t^{n+1} - t^n$ where the superscript denotes the time level. Here, the standard definition of semi-implicit is used where some of the terms in the equations are treated implicitly and some terms explicitly. The distance through the time interval is given by the weight θ. Then the free surface equation becomes

$$\frac{\eta^{n+1} - \eta^n}{\Delta t} + \nabla \cdot \left[\theta\left(\int_h^\eta \mathbf{u}^{n+1} dz\right) + (1-\theta)\left(\int_h^\eta \mathbf{u}^n dz\right)\right] = 0 \tag{5}$$

The material derivative in the momentum equation can be approximated in a number of ways. One possibility is to use an explicit approximation for the advection terms so that stability is then dependent on the Courant number $(Cr = u\Delta t/l_e)$, where u is the current speed normal to an edge and l_e is an element edge length. In previous work this term has been approximated using semi-Lagrangian methods which take advantage of the simplicity of Eulerian methods and the enhanced stability and accuracy of Lagrangian methods (Staniforth and Cøté, 1991).

For simplicity in this discussion, this term is discretized using Eulerian–Lagrangian methods (ELM) rather than semi-Lagrangian methods (SLM). With ELM, only the term at time level n in the material derivative is evaluated at the foot of the trajectory. This is a two step procedure where the material derivative is treated in a Lagrangian sense, and the remainder of the equation is treated in an Eulerian sense at the vertices. With SLM, all terms evaluated at time level n are evaluated at the foot of the trajectory so the entire equation is treated in a Lagrangian sense. Usually there are small differences in the approaches, except where the sea level gradient is large.

Then the momentum equation becomes

$$\frac{\mathbf{u}^{n+1} - \mathbf{u}^*}{\Delta t} - \frac{\partial}{\partial z}\left(A_v \frac{\partial \mathbf{u}^{n+1}}{\partial z}\right) + f\hat{\mathbf{z}} \times \mathbf{u}^n = -g\nabla[\theta\eta^{n+1} + (1-\theta)\eta^n] + \nabla \cdot (A_h \nabla \mathbf{u}^n) \tag{6}$$

where the superscripts $n+1$ and n denote variables evaluated at the fixed nodes in the Eulerian grid at times t^{n+1} and t^n, respectively. At each time step, the velocity is integrated backwards with respect to time to determine where a particle needs to start at time t^n in order to arrive at a grid node at time t^{n+1}. This point is referred to as the foot of the trajectory (Staniforth and Cøté, 1991). The superscript $*$ denotes a variable evaluated at the foot of the trajectory. The material derivative, the first term, thus has a very simple form.

The proper choice of tracking and interpolation methods is critical for maintaining accuracy with SLM and ELM approximations (Casulli, 1987; Staniforth and Côté, 1991). Linear interpolation tends to be highly diffusive (McCalpin, 1988). Although higher-order methods are well established for structured grids with regular quadrilaterals, they are difficult to implement on unstructured grids (Staniforth and Côté, 1991; Le Roux et al., 1997). A recently proposed global-quadratic interpolation method provides a significant step in introducing accurate and efficient SLM and ELM to unstructured grids. Here, a power-series approach in time is used to calculate the trajectory and the global-quadratic interpolation method is used to evaluate the velocity at the foot of the trajectory (Walters et al., 2008).

Note that the vertical viscosity term is treated implicitly to remove stability constraints whereas the horizontal viscosity term is treated explicitly to avoid the solution of a large matrix equation. This introduces a stability constraint that is generally not important. In the remaining discussion, the horizontal stress term will be neglected.

The Coriolis term requires some special attention. Treating this term explicitly such as in (6) is unconditionally unstable. On the other hand, treating this term implicitly leads to the solution a large set of coupled equations which may reduce the efficiency of the model significantly. As an alternative, this term can be integrated in time using some essentially explicit schemes which have the advantage of being both stable and explicit (Durran, 1991; Walters et al., 2009). Hence, a large matrix for velocity does not need to be inverted in the semi-implicit approximation. In the results presented here, we use both implicit and 3rd-order Adams-Bashforth schemes.

2.3. Space discretization

Both the continuity equation and free surface equation reduce to a finite volume approximation for the FD and FE methods described here. With the hydrostatic approximation, the continuity equation is a diagnostic equation for vertical velocity and is not considered further. The free surface equation and momentum equation are treated next.

There is a fundamental difference between FD and FE discretizations. With FD methods, the dependent variables are defined at discrete points in space. For instance, the FD-CC scheme is based on locating the elevation variable at the cell circumcenter and the velocity variable at the midpoint on an edge. The gradient operator is then defined by a stencil that uses local values of the dependent variables. With FE methods, the dependent variables are defined over all space by defining time-dependent nodal values and interpolating these values over space. For the FE discretization used here, the elevation variable is defined at all points in an element as a piecewise constant function. Likewise the velocity variable is defined at all points in an element and the normal component is constant along each edge.

For these staggered grids, there is one degree of freedom for sea level η on each cell and one degree of freedom for the normal component of velocity u_n on each edge. Hence it is more convenient to express the momentum equation in terms of the normal velocity component. Since (6) is invariant under solid rotation in the horizontal plane, the momentum equation for the normal velocity component can be written

$$\frac{u_n^{n+1}-u_n^*}{\Delta t}-\frac{\partial}{\partial z}\left(A_v\frac{\partial u_n}{\partial z}^{n+1}\right)-fu_t^n=-g\frac{\partial \eta^{n+\theta}}{\partial n} \tag{7}$$

where u_n is the normal component of velocity positive outwards, u_t is the tangential component of velocity positive in a counter-clockwise sense around each element, the superscript denotes the time level, $\eta^{n+\theta}=\theta\eta^{n+1}+(1-\theta)\eta^n$, and $\partial/\partial n$ is the gradient operator normal to the cell edge. The treatment of the Coriolis term differs significantly between the FD and FE formulations and is discussed in a separate section. Note that horizontal friction is neglected because it is usually small compared to vertical friction. If it is included, the discretization follows standard methods for FD (Casulli and Walters, 2000) and FE approaches.

After the momentum equation is discretized, it takes the general form

$$\mathsf{M}\left(\frac{\mathsf{U}^{n+1}-\mathsf{U}^*}{\Delta t}\right)+\mathsf{C}\mathsf{U}^n+\mathsf{G}\mathsf{E}^{n+\theta}+\mathsf{T}^v\mathsf{U}^{n+1}=0, \tag{8}$$

where the matrices M, C, G, and T^v, are the velocity mass matrix, Coriolis matrix, gradient matrix, and vertical stress matrix, respectively, U is the vector of velocities, and E is the vector of sea level values. Note that the Coriolis term is explicit but is not treated entirely at time level n because the forward Euler method is unconditionally unstable for inviscid flows. These matrices are given below for the FD and FE schemes.

2.3.1. FD methods

The free surface equation can be derived in the FD context by assuming that the value for η represents a cell average. Moreover, the dependent variable for velocity is defined by the normal velocity component on a cell edge and is assumed to be an edge average. The free surface equation is then directly discretized in finite volume form as

$$A_e\frac{\eta_e^{n+1}-\eta_e^n}{\Delta t}=-\theta\sum_{i=1}^{N_{es}}l_i\left(\int_H u_n^{n+1}dz\right)-(1-\theta)\sum_{i=1}^{N_{es}}l_i\left(\int_H u_n^n dz\right) \tag{9}$$

where subscript $e=1,\ldots,N_e$ denotes the index for a specific cell, N_e is the number of cells, A_e is the area of the cell in the x–y plane, l_i is the edge length of side i, N_{es} is the number of cell sides, and a suitable convention is used to determine normal direction uniquely (Casulli and Walters, 2000). In this study, we will assume $N_{es}=3$ (triangles).

For the FD-CC approximation, η is defined (discretized) at the circumcenter of a computational cell (Casulli and Walters, 2000). Normal velocity is defined at the intersection of the cell edge and the line joining the adjacent circumcenters (Fig. 1). By construction, these lines are perpendicular. The pressure gradient in the momentum equation is then the difference in values at the adjacent circumcenters divided by the distance between circumcenters δ_e.

Note this scheme places constraints on the element shape. All angles of the triangle must be acute or the circumcenter will lie outside the cell making the gradient discretization invalid at best. For an edge joining two right triangles, $\delta_e=0$ and the pressure gradient is either undefined or singular. Similar orthogonal grid constraints exist for quadrilateral cells (Casulli and Walters, 2000).

The orthogonality requirement places severe restrictions on the quality of the grids. Typically if this requirement is not adhered to, the accuracy of the solution can be degraded in comparison with the RT_0 formulation. In fact convergence is not guaranteed for non-orthogonal grids. In addition the calculation of the tangential

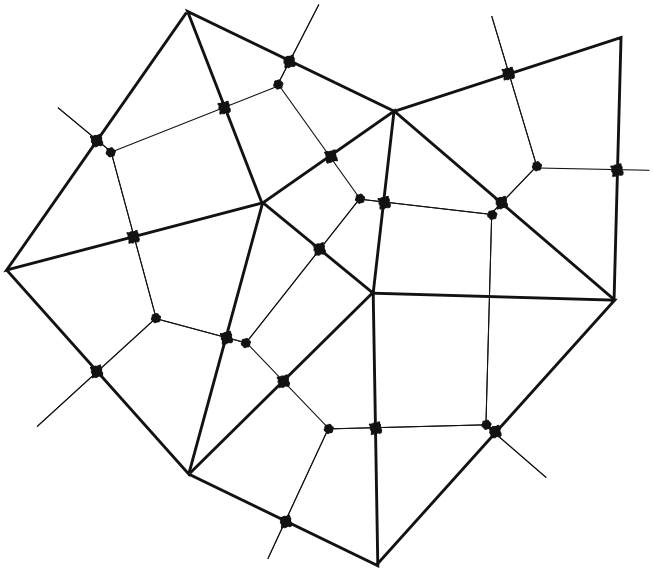

Fig. 1. Definition of an orthogonal grid.

velocities has to be done with care in a circumcenter based scheme. So long as skew-symmetry of the Coriolis matrix is maintained a stable solution is guaranteed.

For a regular grid of rectangles or equilateral triangles, the method is second-order accurate at the circumcenter. As the grids are distorted, the accuracy decreases. Hence the correct strategy for building grids for this approximation is to use a regular element shape as much as possible and grade the elements smoothly to fit a given geometry.

The momentum equation then becomes

$$\frac{Du_n}{Dt} - \frac{\partial}{\partial z}\left(A_v \frac{\partial u_n}{\partial z}\right) = -g\left(\frac{\Delta\eta}{\delta_e}\right) + fu_t + \nabla\cdot(A_h \nabla u_n) \tag{10}$$

where $\Delta\eta$ is the difference in η between the two cells adjacent to an edge, δ_e is the distance between circumcenters adjacent to an edge, and u_t is the tangential velocity component defined in a counter clockwise sense around each cell. Note that there is no equation for u_t so that it must be reconstructed from known values of u_n. The approximation for u_t is discussed in the section on Coriolis approximation.

From (10), the velocity mass matrix M is the identity matrix with unity on the diagonal and zero elsewhere. This is a typical result for FD dscretizations and differs substantially from the FE approximation.

With the FD approximation of the Coriolis term, u_t must be reconstructed from known values of u_n. One such method was proposed by Perot (2000). However, Ham et al. (2007) and Kleptsova et al. (2009) show that this problem is far from simple. Hence a more complete treatment of this term is deferred to a separate section.

The pressure gradient term $\mathsf{GE}^{n+\theta}$ has the form $g\Delta\eta^{n+\theta}/\delta_e$ on each edge (Casulli and Walters, 2000). Because the sea level values are defined at the circumcenters of the two cells adjacent to an edge, the length scale for the gradient is just the distance between circumcenters, δ_e. As will be seen in the next subsection, the distance is imposed in a different manner with FE methods.

The vertical derivatives in the stress term in (10) are discretized using standard cell-centered differences which leads to a tridiagonal matrix at each velocity node. The vertical stress matrix T^v is then block tridiagonal with matrix elements given in Casulli and Walters (2000).

The momentum equations can then be written in a more compact matrix form as

$$\mathbf{A}\mathbf{u}_n^{n+1} = \mathbf{G} - \frac{g\theta\Delta t}{\delta_e}\Delta\eta^{6n+1}\mathbf{Z} \tag{11}$$

where **A** is a block tridiagonal matrix, $\mathbf{u}_n$ is the vector of normal velocity on each edge, **Z** is a vector of depth increments, $\Delta\eta$ is a vector of the difference in cell values, and **G** is a vector of the explicit terms (Casulli and Walters, 2000). The tridiagonal matrix at each velocity node can be inverted and u_n^{n+1} substituted into the free surface Eq. (9) to derive a discrete form of a wave equation that has only η at the $n+1$ time level. Typically, η^{n+1} is solved for first, followed by a calculation of $\mathbf{u}_n^{n+1}$ from (11). This method provides an efficient means to solve the equations. The specific forms of the matrices are shown in detail in Casulli and Walters (2000).

Another discretization based on centroids was developed by Yeh (1981) and called the Integrated Compartment Method (ICM). The dependent variable for sea level is defined as a cell average that is located at the centroid. Normal velocity is defined at the midpoint on cell edges. The free surface equation is developed in the same manner as (9). In the momentum equation, the gradient is defined as the difference between centroid values in the cells adjacent to an edge, divided by the distance between centroids measured perpendicular to the edge in each cell. This approach avoids convergence problems that occur when the centroids are connected directly and thus avoids the cell distortion constraints inherent in the circumcenter scheme. Moreover, this method of calculating gradients is equivalent to the FE approach with the RT_0 element when using node point integration (NPI) as a method of mass lumping.

2.3.2. FE methods

The FE method starts with the choice of an approximation for the dependent variables. The approximation is composed of time-dependent nodal values that are interpolated over space using suitable interpolation functions. The dependent variables in (1) and (2) are expressed in terms of these approximations which gives rise to a residual or error for each equation because the approximation does not satisfy the equations exactly. The residuals are then weighted with test functions (the same as the approximation function using Galerkin's method), integrated over all space, and the weighted residual equations are set to zero. This procedure results in N equations in N unknowns and in effect is a least-squares approximation of the dependent variables. The details for these methods and the appropriate functional spaces are described in many references (Pinder and Gray, 1977; Hanert et al., 2005, 2009) and are not repeated here. The development of the discrete equations for the RT_0 element are found in Hanert et al. (2003) for the 2D equations and Miglio et al. (1999) for the 3D equations.

For the FE spatial discretization, the horizontal domain is divided into triangular elements. Then vertical lines are drawn from each vertex in the grid. The nodes along the verticals are placed according to the vertical discretization desired- σ-coordinates, z-coordinates, or hybrid coordinates. The three-dimensional elements are then pie shaped.

The FE approximation in the horizontal plane uses the Raviart–Thomas element of lowest order (RT_0) where η is approximated as a piecewise constant function on each element, and the normal velocity is approximated as a constant on each edge and varies linearly within the element (Fig. 2, left panel). In the vertical, linear interpolation is used with the nodes located at the mid-point of the element edges. Thus the 3D approximation function is a tensor product between the horizontal interpolation and the vertical interpolation functions.

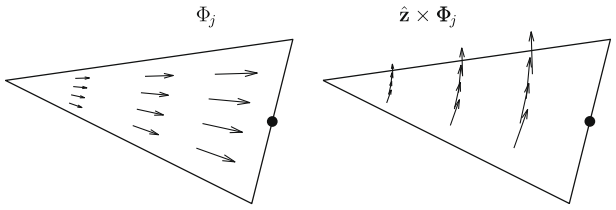

Fig. 2. RT_0 basis functions used to compute the velocity (left) and "perpendicular" velocity used in the Coriolis term (right).

Define $\phi(x,y)$ as the piecewise constant approximation functions for sea level, and $\mathbf{\Phi}(x,y)$ as the horizontal approximation functions (vector) and $\zeta(z)$ as the vertical approximation functions for normal velocity. Then $\phi_i = 1$ on element i and 0 otherwise. The horizontal approximation functions are

$$\mathbf{\Phi}_i = \frac{\mathbf{x} - \mathbf{x}_i}{2A_e/l_i}$$

where $\mathbf{x}_i$ is the vertex location opposite to edge i, $2A_e/l_i$ is the height of the triangle from edge i, and A_e is the area of the element (Fig. 2). The vertical approximation functions are

$$\zeta_k = \begin{cases} \frac{z - z_{k-1}}{z_k - z_{k-1}} & \text{for } (z_{k-1} \leqslant z \leqslant z_k) \\ \frac{z_{k+1} - z}{z_{k+1} - z_k} & \text{for } (z_k \leqslant z \leqslant z_{k+1}) \end{cases}$$

Then sea level and velocity are interpolated as

$$\eta \approx \eta^h = \sum_{e=1}^{N_e} \eta_e \phi_e$$

$$\mathbf{u} \approx \mathbf{u}^h = \sum_{j=1}^{N_s} \sum_{k=1}^{N_v} u_{jk} \mathbf{\Phi}_j \zeta_k$$

where superscript h denotes an approximation, η_e is the value for sea level on element e, u_{jk} is the normal velocity on edge j and level k as a generalized scalar nodal value, N_e is the number of elements, N_s is the number of sides, and N_v is the number of nodes in the vertical.

The weighted residual form (weak formulation) can be written as (Miglio et al., 1999; Hanert et al., 2003)

$$\int_\Omega L_1(\eta^h, \mathbf{u}^h)\phi d\Omega = 0 \tag{12}$$

$$\int_\Omega \int_H \mathbf{L}_2(\eta^h, \mathbf{u}^h) \cdot \mathbf{\Phi} \zeta dz d\Omega = 0 \tag{13}$$

where L_1 is the free surface equation (4), $\mathbf{L}_2$ is the momentum equation (2), and Ω is the horizontal spatial domain.

The free surface equation (4) is then written as

$$\int_\Omega \frac{\partial \eta^h}{\partial t} \phi_i d\Omega = -\int_\Omega \nabla \cdot \left(\int_h^\eta \mathbf{u}^h dz \right) \phi_i d\Omega \quad \forall i = 1, \ldots, N_e \tag{14}$$

Because η is approximated as a piecewise constant function on each element, the free surface equation becomes

$$\begin{aligned} A_e \frac{\eta_e^{n+1} - \eta_e^n}{\Delta t} &= -\theta \int_{\Gamma_e} \left(\int_H u_n^{n+1} dz \right) d\Gamma_e - (1-\theta) \int_{\Gamma_e} \left(\int_H u_n^n dz \right) d\Gamma_e \\ &= -\theta \sum_{i=1}^{Nes} l_i \left(\int_H u_n^{n+1} dz \right) - (1-\theta) \sum_{i=1}^{Nes} l_i \left(\int_H u_n^n dz \right) \end{aligned} \tag{15}$$

where Γ_e is the boundary of the element and the last term has been converted from a volume divergence to a surface integral using the Gauss Divergence Theorem. Note that this approximation is identical to (9) for the FD method.

The momentum equation is also treated using standard Galerkin FE methods. The weighted residual statement for the momentum Eq. (13) can be written in the form of (8) where

$$\mathsf{M}_{ijkl} = \int_\Omega \mathbf{\Phi}_j \cdot \mathbf{\Phi}_i \int_H \zeta_l \zeta_k dz d\Omega$$

$$\mathsf{C}_{ijkl} = \int_\Omega f(\hat{\mathbf{z}} \times \mathbf{\Phi}_j) \cdot \mathbf{\Phi}_i \int_H \zeta_l \zeta_k dz d\Omega$$

$$\mathsf{G}_{ijk} = -g \int_\Omega \phi_j \nabla \cdot \mathbf{\Phi}_i \int_H \zeta_k dz d\Omega + g \int_{\partial\Omega} (\boldsymbol{\phi}_j \mathbf{\Phi}_i) \cdot \hat{\mathbf{n}} \int_H \zeta_k dz d\Omega$$

$$\mathsf{T}^v_{ijkl} = \int_\Omega \mathbf{\Phi}_j \cdot \mathbf{\Phi}_i \int_H \frac{\partial \zeta_l}{\partial z} A_v \frac{\partial \zeta_k}{\partial z} dz d\Omega - \int_\Omega [\gamma \mathbf{\Phi}_j \cdot \mathbf{\Phi}_i \zeta_l \zeta_k]_h^\eta d\Omega$$

Note that the pressure gradient and vertical stress terms are integrated by parts so that extra terms for the boundary integral of sea level and surface and bottom stress appear. These terms are useful for applying boundary conditions.

The two most significant differences between the FD and FE formulation are the form of the mass matrix M and the Coriolis term $\mathsf{C}\mathbf{U}^n$. The mass matrix is composed of a horizontal part which has five (triangles) or seven (quadrilaterals) non-zero entries for each equation corresponding to the edges in the two adjacent elements which form the support for a particular edge. The vertical part is a tridiagonal matrix. Hence the structure is block tridiagonal matrices arranged in 5 or 7 diagonals. This structure differs markedly from the FD case where the horizontal part is the identity matrix and leads to a much higher computational expense for the FE matrix solution.

With the FE approximation, the Coriolis term is expressed directly in terms of the interpolation functions and the normal velocity on the edges. The element matrix is a fully-populated 3×3 matrix. When assembled into the global matrix, the Coriolis term has 5 diagonals (triangles) or 7 diagonals (quadrilaterals) reflecting the local support from the 2 adjacent triangles to an edge.

The pressure gradient term is trivial to integrate because the horizontal part is constant on each element. Then

$$\mathsf{GE}^{n+\theta} = g\Delta t \Delta \eta^{n+\theta} \mathbf{Z} + B^{n+\theta} \tag{16}$$

where B are the boundary terms and $\mathbf{Z}$ is a vector with elements $Z_k = \int_H \zeta_k dz$. Note that there is no length scale δ_e such as with the FD scheme. The effective length scale is determined by the horizontal part of the mass matrix instead. If we write $\mathsf{N} = \int_\Omega \mathbf{\Phi}_j \cdot \mathbf{\Phi}_i d\Omega$, then the length scale is related to N^{-1}. For the full mass matrix (FE-FM), there is no readily identifiable length because the inverse matrix is in general fully populated. For the mass lumping scheme proposed by Baranger et al. (1996) (FE-CC here), the diagonal contains the distance between circumcenters. Hence the pressure gradient term is identical to the FD-CC scheme. For the mass lumping scheme where the normal distance to the centroid is used (FE–NPI), the effective length is the same as that proposed in the ICM method.

In the vertical, the FD-CC and FE-CC (Miglio et al., 1999) schemes use face centered velocity locations. The vertical component of stress is solved using standard FD stencils and the boundary conditions are applied with virtual points located outside of the boundary. The other FE schemes along with another version of FE-CC use edge centered velocity locations with a linear variation within each element. A linear variation is required to approximate the vertical stress term when it is integrated by parts. An added benefit is that the boundary conditions arise in a natural way from the boundary integrals.

After some manipulation, the FE momentum Eq. (2) can be written in the same compact form as (11)

$$\mathbf{A}\mathbf{u}_n^{n+1} = \mathbf{G} - g\theta\Delta t \Delta \eta^{n+1} \mathbf{Z} \tag{17}$$

where

$$\mathbf{A} = (\mathsf{M} + \mathsf{T}^v)$$

$$\mathbf{G} = (\mathsf{M}\mathbf{u}_n^* - \Delta t \mathsf{C}\mathbf{u}_n^m) - (1-\theta) g \Delta t \Delta \eta^n \mathbf{Z} + \mathbf{B}$$

$$\mathbf{Z} = \int_H \zeta dz$$

where $\Delta\eta^n$ is the difference between element values adjacent to the edge, the Coriolis term is evaluated at time level m, and **B** are boundary terms that arise from the integration by parts of the the horizontal sea level gradient terms.

In general, **A** is a large sparse matrix that is block tridiagonal at each velocity node in the horizontal grid. There are several options for solving this system. First, one could solve the full matrix as a coupled system with the free surface equation (FM scheme). This is the least efficient procedure but potentially the most accurate. Second, one could solve the matrix by diagonalizing this matrix in the horizontal. The solution would then involve solving a tridiagonal matrix at each velocity node, substituting for u_n^{n+1} in the free surface Eq. (9), and solving a discrete wave equation as described for the FD-CC scheme. Thus the FD and FE scheme would have essentially the same efficiency.

Several methods are available to diagonalize the mass matrix (Baranger et al., 1996; Le Roux et al., 2008). One mass lumping method was originally proposed by Baranger et al. (1996) and subsequently used by Miglio et al. (1999) and for the FE-CC scheme in this paper. The velocity mass matrix N is approximated as

$$\mathsf{N}_{ij}^{lumped} = d_i \delta_{ij},$$

where d_i is the distance between the circumcenters of the two triangles sharing the edge i and δ_{ij} is the Kronecker delta. Essentially, this scheme reproduces the circumcenter FD-CC scheme described in the previous subsection without the need to reconstruct u_t. Another method is to approximate the velocity mass matrix N for triangular elements as

$$\mathsf{N}_{ij}^{lumped} = \frac{2A_i}{3l_i}\delta_{ij},$$

where A_i is the sum of the area of the two elements adjacent to side i. This scheme is denoted as FE–NPI and produces a diagonal matrix where the diagonal contains values for the distance between element centroids as measured perpendicular from the edge (Walters and Casulli, 1998; Walters, 2005). Other methods are possible but we have not tried them.

3. Coriolis discretization

A distinctive feature of these staggered grid methods is that the dependent variables are the normal component of the velocity at each cell edge and the sea level (pressure) at cell centers. Hence if the full velocity vector is required, such as in the calculation of the Coriolis acceleration, the component of velocity tangential to the cell face must be calculated at that cell face. This is true in both the structured grid (Arakawa C-grid) and unstructured grid cases.

Espelid et al. (2000) showed that in the calculation of the tangential velocities in structured C-grid models, it was important that the interpolation matrices were skew symmetric or similar to skew symmetric (see eg Strang (1988)). They also demonstrated that an energy conserving C-grid discretisation for the Coriolis term could be achieved if the weights in the interpolation matrix were chosen such that the semi-discrete system matrix is similar to a skew symmetric matrix. Perot (2000) considered the case of unstructured grid schemes for the solution of the two-dimensional Navier–Stokes equations in a non-rotating frame of reference, in domains with a constant depth. He presented energy conservative discretisation methods. Ham et al. (2007) showed that many straightforward discretisations are subject to instability. They demonstrated that a symmetry preserving interpolation was essential in maintaining stability. In addition, skew symmetry could not be achieved in the case of extended centroid based schemes where the sea level gradient is approximated over several cells rather than the adjacent cells. As the pressure gradient stencil is increased, the skew symmetric properties cannot be maintained in general.

3.1. FD approximation

The FD-CC approach requires a reconstruction for u_t from the known values of u_n. The interpolation consists of two stages. In the first step the full velocity vector in the cell interior is reconstructed out the normal velocity components of the cell faces. Then in the second step this velocity vector is projected back to the cell face tangent direction. This results in two values for the tangential velocity component at each cell face. Therefore the reconstructed tangential velocity component is a cell-weighted linear combination of these two values. Note that in the following development, (u_i, v_i) are the normal and tangential components of velocity on edge i, not the cartesian components in the (x,y) directions.

One of the possible velocity reconstructions in a polygon was presented by Perot (2000). This can be expressed using the position of the circumcenter. In the case of a triangle this is given by:

$$A_c\mathbf{u} = u_i l_i d_i^c \mathbf{n}_i + u_j l_j d_j^c \mathbf{n}_j + u_k l_k d_k^c \mathbf{n}_k \tag{18}$$

where A_c is the cell area, u_i is the normal velocity at face i and l_i is length of face i, with d_i^c the orthogonal distance of the circumcenter to face i, with similar definitions for cell faces j and k. For the projection in the tangential direction of face i the unit vector $\mathbf{t}_i$ is employed. Therefore the reconstructed tangential velocity is given by:

$$v_i = \frac{d_j^c l_j}{A_c} u_j \mathbf{n}_j \cdot \mathbf{t}_i + \frac{d_k^c l_k}{A_c} u_k \mathbf{n}_k \cdot \mathbf{t}_i \tag{19}$$

This is the tangent velocity to face i in triangle a, however, we have another value at face i reconstructed in the adjacent triangle b. Therefore a linear combination may be constructed so that, $v_i = \gamma_i^a v_i^a + \gamma_i^b v_i^b$, where γ_i^a and γ_i^b are weights. In the case of constant depth $\gamma_i^a + \gamma_i^b = 1$, and $\gamma_i^a = d_i^a/d_i$ and $\gamma_i^b = d_i^b/d_i$ satisfies the skew symmetry property of the system matrix. However, in the case of variable bathymetry this reconstruction fails to satisfy the skew symmetry property and has to be modified. Ham et al. (2007) suggested the choice $\gamma_i^a = (d_i^a h_a)/(d_i h_i)$ and $\gamma_i^b = (d_i^b h_b)/(d_i h_i)$. This can be written in terms of the sum of fluxes around a cell,

$$v_i = \sum_c \sum_f \frac{h_i d_i^c d_f^c l_f}{h_i d_i A_c} u_f \mathbf{n}_f \cdot \mathbf{t}_i \tag{20}$$

where the outer sum goes over the cells c sharing face i, while the inner summation goes over the faces f surrounding cell c, d_f^c is the distance between the face f and cell c circumcenter, l_f is the length of face f, h_c is the cell depth at the circumcenter, h_i is the depth at the face i. However, Kleptsova et al. (2009) recently demonstrated that a more consistent and accurate method is obtained by taking into account the depth integrated continuity equation, hence they propose,

$$v_i = \sum_c \sum_f \frac{h_f d_i^c d_f^c l_f}{h_c d_i A_c} u_f \mathbf{n}_f \cdot \mathbf{t}_i \tag{21}$$

The velocity reconstruction method leads to a piecewise constant approximation of u_t at cell circumcenters. This reconstruction maintains the skew symmetric and conservation properties of the Coriolis matrix. Other methods of reconstruction such as projecting the velocity on a P_1 basis either globally or locally do not in general result in a Coriolis matrix that is skew symmetric.

For the centroid based methods such as ICM (Yeh, 1981), Ham et al. (2007) indicate that it is not possible to create a Coriolis discretization with the proper skew symmetric properties except on a

regular grid where the centroid and circumcenter are at the same location.

3.2. FE approximation

The Coriolis term is expressed in terms of the element bases and u_n in (8) using a standard FE approximation. The "perpendicular" velocity component used in the Coriolis term ($\hat{\mathbf{z}} \times \mathbf{u}$) is computed by using the basis functions ($\hat{\mathbf{z}} \times \mathbf{\Phi}_j$). This component is defined in each element such that it is perpendicular to the approximation $\mathbf{u}^h$. Hence in order to compute the Coriolis term with RT_0, we actually modify the set of basis functions rather than develop nodal values for a tangential velocity component. Both basis functions are shown in Fig. 2.

Hence in the momentum equation, the Coriolis matrix C takes the following form:

$$C_{ij} = \int_\Omega f \mathbf{\Phi}_i \cdot (\hat{\mathbf{z}} \times \mathbf{\Phi}_j) d\Omega = \int_\Omega f \mathbf{\Phi}_j \cdot (\mathbf{\Phi}_i \times \hat{\mathbf{z}}) d\Omega$$
$$= -\int_\Omega f \mathbf{\Phi}_j \cdot (\hat{\mathbf{z}} \times \mathbf{\Phi}_i) d\Omega$$

which shows that the Coriolis matrix is naturally skew symmetric. As a result, the eigenvalues of the Coriolis matrix are all purely imaginary (Fig. 3). It should be noted that the FE method does not require a reconstruction of the tangential velocity as the Coriolis term is directly computed from the normal velocity nodal values. This removes the ambiguities associated with determining a method used to compute the tangential velocity from the normal velocity.

4. Properties

4.1. Phase accuracy

The complex propagation factor was introduced by Leendertse (1967) as a tool for assessing the accuracy of numerical schemes used with waves. The propagation factor is the ratio of the complex amplitude of the computed wave and that of the analytical wave after the analytical wave propagates one wavelength. Then the magnitude of the propagation factor is the ratio of the amplitude of the waves and provides information on numerical damping. The argument of the propagation factor describes the relative phase speed between the two waves.

The analytical dispersion relation and the discrete dispersion relation obtained from the space-discretized and time-continuous equations for the RT_0 element have been derived by Le Roux et al. (2007) for inertia-gravity waves and Le Roux and Pouliot (2008) for Rossby waves. Here we present the discrete dispersion relation derived from the argument of the amplification factor using the fully discretized equations and following the methods of Bernard et al. (2008). To obtain these results, a semi-implicit time integration scheme has been used so that for $\theta = 0.5$ the magnitude of the propagtion factor is unity and is not shown here.

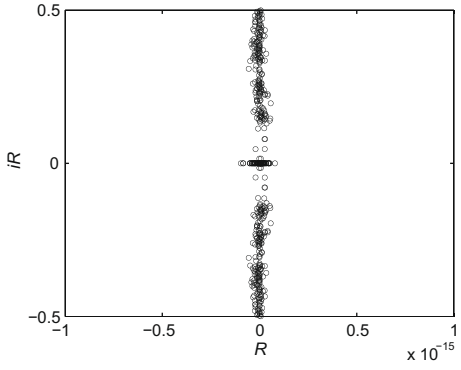

Fig. 3. Eigenvalues spectrum of the Coriolis matrix C. It can be seen that the eigenvalues are all purely imaginary. The matrix has been computed on an unstructured mesh of $[0,1] \times [0,1]$ composed of 256 elements.

All the dispersion analysis have been performed on an unstructured mesh with an average of 12 elements along the x- and y-directions. The domain is assumed periodic along the x-direction and bounded in the y-direction (solid boundaries).

The linear rotating shallow water equations have been used with the following physical parameter values: water depth $H = 1000$ m, Coriolis parameters $f_0 = 3 \times 10^{-4} \mathrm{s}^{-1}$ and $\beta = 10^{-11}$ $(\mathrm{ms})^{-1}$, gravitational acceleration $g = 10 \mathrm{ms}^{-2}$ and the domain extent is $L \times L$, where $L = 10^6$ m. A β-plane approximations is used where $f = f_0 + \beta y$. When computing the dispersion relation and amplification factor of inertia-gravity waves, we assume $\beta = 0$. The time step has been selected so that the gravity wave CFL number is equal to 0.2.

The approximations that are compared here include FE–FM, a solution of the full mass matrix; FE-CC, lumped mass matrix with the distance between circumcenters on the diagonal; FE–NPI, lumped mass matrix with the distance between centroids on the diagonal; and FD-CC, the finite difference circumcenter approach.

The dispersion relation and argument of the amplification factor obtained by using these methods are shown in Fig. 4 for gravity waves and in Fig. 5 for Rossby waves. For gravity waves, the FE–FM scheme has the best accuracy for the dispersion relation. The accuracies of the other schemes are about the same and all would be considered acceptable. For Rossby waves, all the schemes exhibit similar accuracy.

5. Numerical example

The models were applied to a test case for a freely propagating Kelvin wave in a circular basin (Ham et al., 2007). The basin is 250 km in radius, is 5 m in depth, uses an f plane approximation with f estimated at 45 degrees, and has an initial velocity and sea level specified. The two-dimensional linear shallow water equations are used where depth is constant in the continuity equation, and there are no friction or advection terms. The time step used was 20 min. The initial conditions are

$$\eta(r,0) = e_0 \exp((r - r_0)/L_D) \cos(\theta)$$
$$u_\theta(r,0) = e_0 (c/h) \exp((r - r_0)/L_D) \cos(\theta)$$
$$u_r(r,0) = 0$$

where u_θ is the tangential component of velocity, u_r is the radial component of velocity, $e_0 = 0.05$ m, r is the radius, $r_0 = 2.5 \times 10^5$ m is the radius of the basin, $L_D = c/f$ is the Rossby radius, $c = \sqrt{gh}$ is phase speed, and $h = 5$ m is water depth.

Although this is a simple test case, it provides a demanding test on numerical methods. First, the problem is inviscid so that any problems with stability that arise are readily apparent (Ham et al., 2007). On the other hand, dissipative methods can be seen by the decrease in amplitude and energy. Approximate analytical solutions (Csanady, 1982) can be used to assess accuracy.

Two grids were used in the tests (Fig. 6). Grid 1 was generated with a frontal marching algorithm (Löhner and Oñate, 1998) using a newer version of the grid generation software developed by Henry and Walters (1993). This grid contains 1304 vertices and 2486 triangular elements and started with 120 nodes spaced evenly around the boundary. Grid 2 is more irregular with 167 points on the boundary and contains 2782 vertices and 5395 triangular elements. Grid 2 is not orthogonal because it contains approximately 100 obtuse triangles.

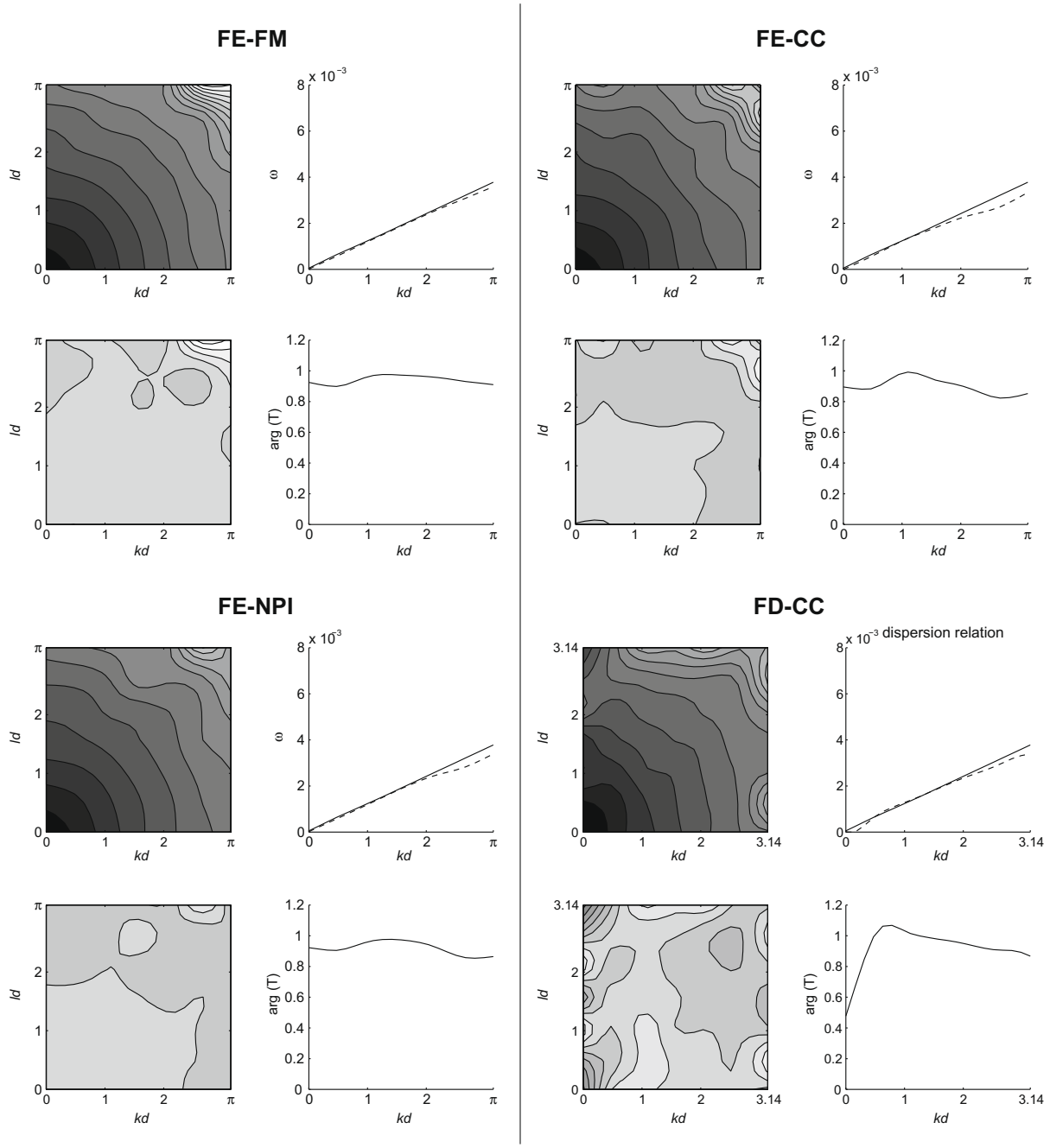

Fig. 4. Dispersion relation (top) and argument of the amplification factor (bottom) obtained for inertia-gravity waves when the velocity mass matrix is lumped with the method proposed by Baranger et al. (1996). For the dispersion relation, the exact solution is shown in solid line and the numerical solution in dashed line.

The FE–FM scheme uses an implicit treatment for all the terms in the equations with a time weight $\theta = 0.5$. Because the full matrix is inverted at each time step, there is no significant increase in runtime by including an implicit treatment of the Coriolis terms. This method represents the most accurate solution of the FE schemes, but is also by far the least efficient.

The FE–NPI scheme uses a semi-implicit treatment for the gravity wave terms and an explicit integration of the Coriolis term using the third-order Adams-Bashforth method (Durran, 1991). The stability of the solution depends on the time weight θ (Walters et al., 2009). For this simulation, $\theta = 0.503$ and the solution remains stable for all the simulations. The efficiency of this scheme is much higher than FE–FM.

The FE-CC scheme uses an implicit treatment for all the terms in the equations with the time weight $\theta = 0.5$. This approach does not make use of the higher efficiency of the lumped mass matrix, but avoids selecting a time approximation for the Coriolis term.

The FD-CC scheme uses a semi-implicit treatment for the gravity wave terms and a split-step integration of the Coriolis term.

Time-series plots of the first few rotations of the wave are shown in Fig. 7 for grid 1 and the results for grid 2 are similar. The 5 points plotted are equidistant points arranged on a north-south line that passes through the center of the basin. Time-series plots near the end of the simulation are shown in Fig. 8 for grid 1 and Fig. 9 for grid 2. Note that FD-CC was not run using grid 2 because the model requires an orthogonal grid. However, FE-CC was run anyway with the results plotted in the figures. The phase errors for FE-CC using grid 2 could be a result of the presence of obtuse triangles.

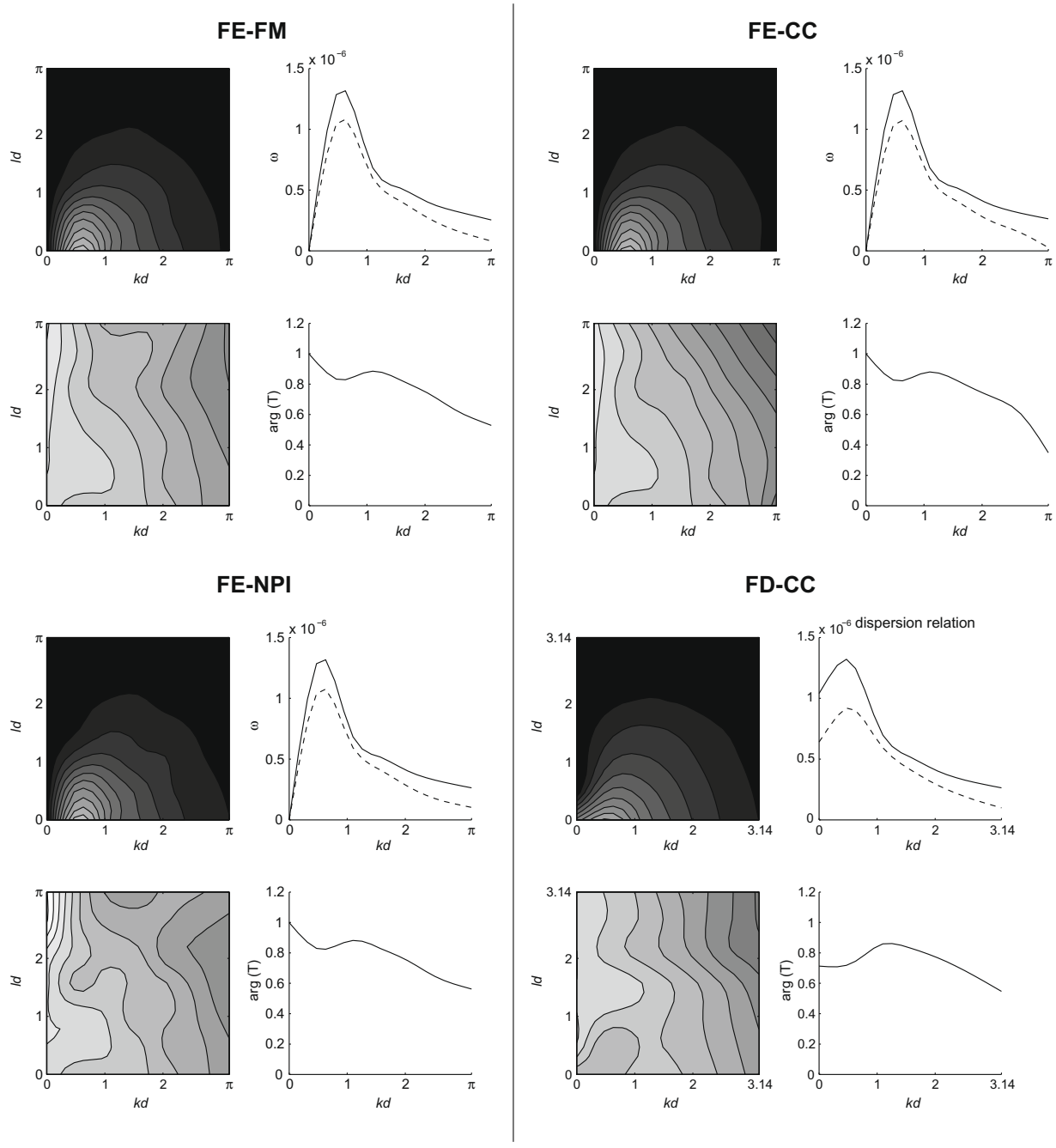

Fig. 5. Same as Fig. 4 except for Rossby waves.

The results are nearly the same on both grids with somewhat noisier results using grid 2. Startup transients are also apparent in the results particularly at the points in mid-basin. The different methods display a different rotation rate for the wave that reflects differences in computed phase speed. During the length of this simulation (5000 steps $\times 20$ min = 10^5 min.), FE–FM completed 31.3 cycles, FE–NPI competed 31.5 cycles, FE-CC completed 31.3 cycles on grid 1 and 31.1 cycles on grid 2, and FD-CC completed 31.4 cycles. The phase errors at the end of the simulation can be seen in Figs. 8 and 9.

In addition, FE–FM, FE–NPI, and FE-CC maintained the initial amplitude of the wave. This suggests that the initial conditions and the numerical approximations were compatible so that the models faithfully reproduced the correct dynamics. The FD-CC scheme suffered a small loss of amplitude suggesting that the approximation for the Coriolis term was not as compatible as the FE schemes. In the course of these experiments with the FE methods, we found that an accurate integration of the Coriolis terms was essential. For the FE–NPI scheme, integrating the Coriolis and mass matrix with the same 3-point quadrature led to 3% phase errors. Using an exact quadrature for the Coriolis term reduced the phase errors to aproximately the same as the other schemes.

Snapshots of the sea level and velocity are shown in Fig. 10. The differences in rotation rate of the waves are apparent.

Dispersion analysis (Le Roux et al., 2008) and numerical results for FE–NPI (Walters, 2005) show that the phase errors are typically less than 1% for well resolved waves. Use of a lumped mass matrix usually results in a smaller phase speed FE-CC (Le Roux et al., 2008) rather that the larger phase speed observed here for FE–NPI. It is not apparent at this time why there is a phase lead with FE–NPI.

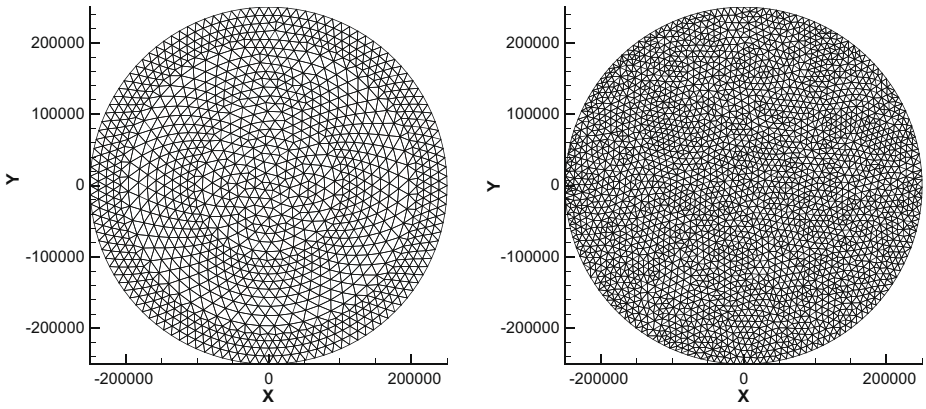

Fig. 6. Grids used in the simulations. Front-generated grid (left) and irregular grid (right).

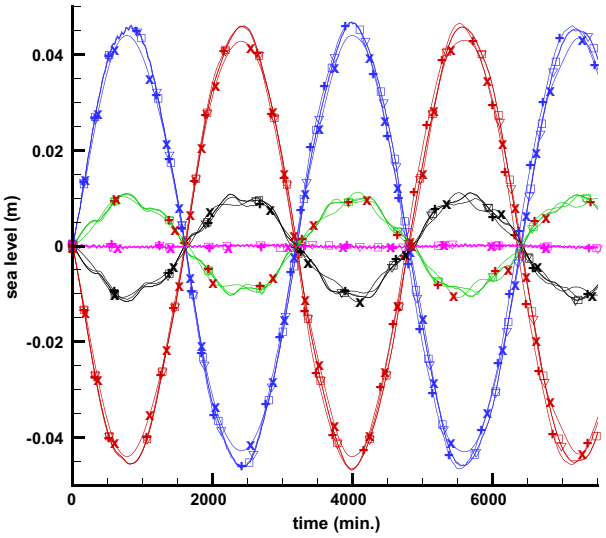

Fig. 7. Time-series data for a north-south line of points with grid 1. FE–FM □, FE-CC ▽, FE–NPI +, FD-CC ×. The points are arranged from north to south (blue,green,violet,black, and red). (For interpretation of the references to color in this figure legend, the reader is referred to the web version of this paper.)

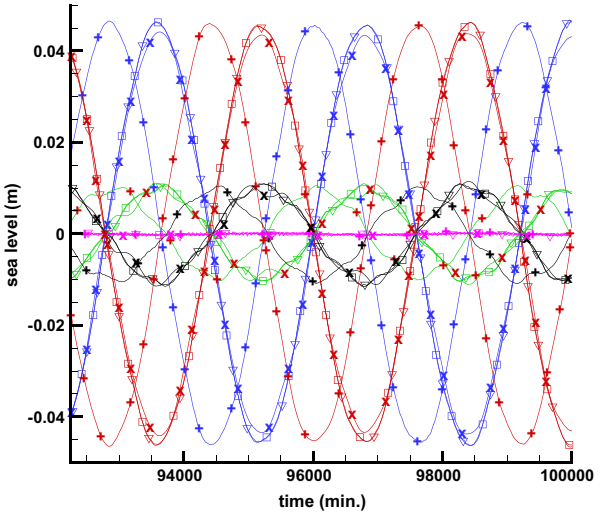

Fig. 8. Time-series data for a north–south line of points with grid 1 near the end of the simulation. Symbols are the same as in Fig. 7.

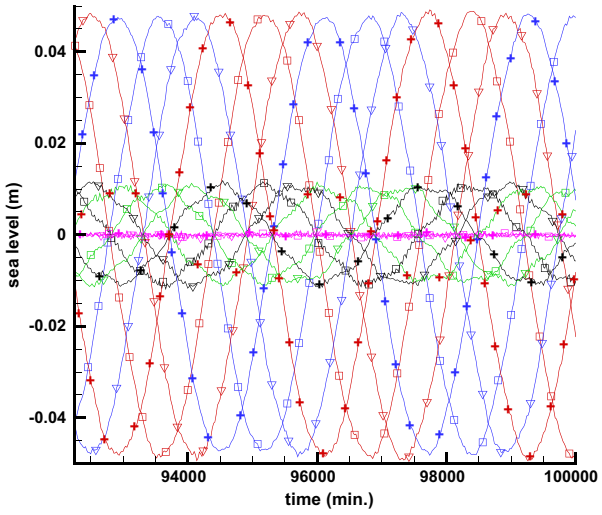

Fig. 9. Time-series data for a north–south line of points with grid 2 near the end of the simulation. Symbols are the same as in Fig. 7.

6. Conclusions

We have examined a class of unstructured, staggered grid models for the shallow water equations where the continuity equation reduces to a finite-volume approximation. The momentum equations can be approximated with finite difference, finite element, or finite volume methods. For reasons stated in the introduction, we have not analyzed the finite volume approach. Of these, the FD-CC approximation using circumcenters and the FE approximation using the RT_0 element seem the most attractive and form the basis for this study.

Each of these methods has advantages and disadvantages. The FD-CC formulation tends to be more efficient but has significant constraints on the grid which is required to be orthogonal (Casulli and Walters, 2000). In addition, the Coriolis term must be treated carefully to maintain skew symmetry (Ham et al., 2007; Perot, 2000; Bonaventura and Ringler, 2005). On the other hand, the FE formulation has no significant constraints on the grid (except FE-CC) and the Coriolis term is treated correctly using the standard FE approximation. The full matrix FE formulation is inefficient compared to the FD-CC and lumped FE schemes due to the presence of a large, sparse mass matrix. The FE formulations which use lumping of the mass matrix, FE-CC and FE–NPI, have equivalent efficiency as the FD-CC scheme. However, FE-CC has the same

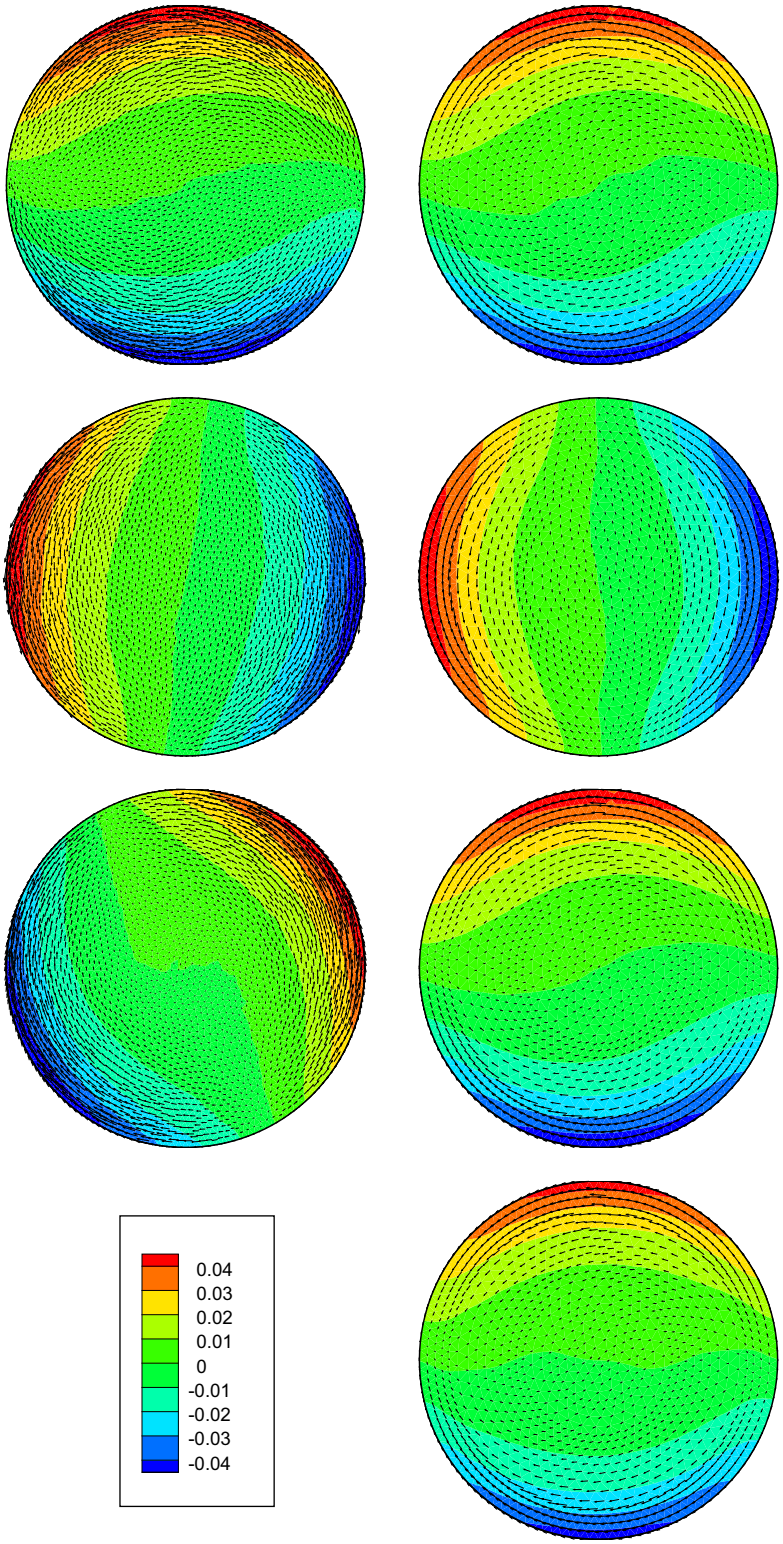

Fig. 10. Results using FE–FM (top), FE–NPI (top–middle), FE-CC (bottom–middle), and FD-CC (bottom) after approximately 31 cycles (10^5 min). Irregular grid (left) and front-generated grid (right). The scale (bottom left) is in meters.

grid constraints as FD-CC since they are both based on a circumcenter approach.

Of these methods, FE–FM seems to have the best phase accuracy, followed closely by FE-CC and FD-CC for regular grids, and then by FE–NPI. For the irregular grid, FE-CC and FE–NPI have about the same phase errors where they lag and lead the FE–FM results, respectively. All these schemes are reasonably accurate. None of the approaches showed significant amplitude errors except FD-CC during the initial period of the test problem. Apparently, the reconstruction of the Coriolis term is not entirely

compatible with the initial condition for a Kelvin wave. The cause for this is unknown at this time.

The choice between methods can be considered in terms of stability, accuracy and efficiency. All these methods are stable as formulated here. FE–FM is the most accurate but the least efficient. FE-CC and FD-CC have much better efficiency with a small loss in accuracy, but are subject to grid constraints. FE–NPI has good efficiency with no grid constraints, but has slightly worse accuracy. In the end, the choice of methods is problem specific and can have more subjective inputs.

With the correct choice of time-stepping procedure for the treatment of the Coriolis term (Walters et al., 2008) as well as the maintenance of a skew-symmetric matrix for spatial interpolation (Ham et al., 2007), the FD and FE unstructured grid formulations presented here all perform well. Moreover, all of these schemes allow a straightforward approach for flooding and drying. This class of FE and FD models is robust, efficient and accurate. They can easily be used in operational forecasting codes as has been successfully shown by Walters et al. (2009) and Lane et al. (2009) for New Zealand.

Acknowledgements

EH thanks the Nuffield Foundation for a newly appointed lecturer award. We are grateful to O. Kleptsova (TUD) who ran the simulations for the FD-CC case.

References

Baranger, J., Maitre, J.F., Oudin, F., 1996. Connection between finite volume and mixed finite element methods. Mathematical Modelling and Numerical Analysis 30, 445–465.

Bernard, P.-E., Remacle, J.-F., Legat, V., Deleersnijder, E., 2008. Dispersion analysis of discontinuous Galerkin schemes applied to Poincaré, Kelvin and Rossby waves. Journal of Scientific Computing 34, 26–47.

Bonaventura, L., Ringler, T., 2005. Analysis of discrete shallow-water models on geodesic Delaunay grids with C-type staggering. Monthly Weather Review 133, 2351–2373.

Bradford, S.F., Sanders, B.F., 2002. Modeling flows with moving boundaries due to flooding, recession, and wave run-up. In: Spaulding, M.L. (Ed.), Estuarine and Coastal Modeling: Proceeding of the Seventh International Conference, ASCE, pp. 695–708.

Casulli, V., 1987. Eulerian–Lagrangian methods for hyperbolic and convection dominated parabolic problems. In: Taylor, C., Owen, D.R., Hinton, E. (Eds.), Computational Methods for Non-linear Problems. Pineridge Press, Swansea, pp. 239–268.

Casulli, V., Walters, R.A., 2000. An unstructured grid, three-dimensional model based on the shallow water equations. International Journal for Numerical Methods in Fluids 32 (3), 331–348.

Casulli, V., Zanolli, P., 2002. Semi-implicit numerical modeling of nonhydrostatic free-surface flows for environmental problems. Mathematical and Computer Modelling 36, 1131–1149.

Chen, C., Liu, H., Beardsley, R.C., 2003. An unstructured, finite-volume, three-dimensional, primitive equation ocean model: Application to coastal ocean and estuaries. Journal of Atmospheric and Oceanic Technology 20, 159–186.

Csanady, G.T., 1982. Circulation in the coastal ocean. Riedel Publ., 279 pp.

Danilov, S., Kivman, G., Schröter, J., 2004. A finite element ocean model: principles and evaluation. Ocean Modelling 6, 125–150.

Denlinger, R.P., Iverson, R.M., 2001. Flow of variably fluidized granular masses across 3D terrain: 2. Numerical predictions and experimental tests. Journal of Geophysical Research 106 (B1), 553–566.

Durran, D.R., 1991. The third-order Adams-Bashforth method: an attractive alternative to Leapfrog time differencing. Monthly Weather Review 119, 702–720.

Espelid, T.O., Berntsen, J., Barthel, K., 2000. Conservation of energy for schemes applied to the propagation of shallow-water inertiagravity waves in regions with varying depth. International Journal for Numerical Methods in Engineering 159, 1521–1545.

Fringer, O.B., Gerrirsen, M., Street, R.L., 2006. An unstructured grid, finite volume, nonhydrostatic, parallel coastal ocean simulator. Ocean Modelling 14, 139–173.

Griffies, S.M., Böning, C., Bryan, F.O., Chassignet, E.P., Gerdes, R., Hasumi, H., Hirst, A., Treguier, A.-M., Webb, D., 2000. Developments in ocean modelling. Ocean Modelling 2, 123–192.

Ham, D.A., Kramer, S.C., Stelling, G.S., Pietrzak, J.D., 2007. The symmetry and stability of unstructured mesh C-grid shallow water models under the influence of Coriolis. Ocean Modelling 16, 47–60.

Hanert, E., Legat, V., Deleersnijder, E., 2003. A comparison of three finite elements to solve the linear shallow water equations. Ocean Modelling 5, 17–35.

Hanert, E., Le Roux, D.Y., Legat, V., Deleersnijder, E., 2005. An efficient Eulerian finite element method for the shallow water equations. Ocean Modelling 10, 115–136.

Hanert, E., Walters, R.A., Le Roux, D.Y., Pietrzak, J., 2009. A tale of two elements: $P_1^{NC} - P_1$ and RT_0. Ocean Modelling 28, 24–33.

Henry, R.F., Walters, R.A., 1993. A geometrically-based, automatic generator for irregular triangular networks. Communications in Applied Numerical Methods 9, 555–566.

Kleptsova, O., Pietrzak, J.D., Stelling, G.S., 2009. On the accurate and stable reconstruction of tangential velocities in C-grid ocean models. Ocean Modelling 28, 118–126.

Lane, E.M., Walters, R.A., Uddstrom, M., 2009. EcoConnect Forecast System with an Unstructured Grid Ocean Model. Ocean Modelling 28, 88–96.

Le Roux, D.Y., Hanert, E., Rostand, V., Pouillot, B., 2008. Effect of mass lumping on gravity and Rossby waves in 2D finite-element shallow-water models. International Journal for Numerical Methods in Fluids, doi:10.1002/fld.1837.

Le Roux, D.Y., Lin, C.A., Staniforth, A., 1997. An accurate interpolating scheme for semi-Lagrangian advection on an unstructured mesh for ocean modelling. Tellus 49 (A2), 119–138.

Le Roux, D.Y., Lin, C.A., Staniforth, A., 2000. A semi-implicit semi-Lagrangian finite-element shallow-water ocean model. Monthly Weather Review 128, 1384–1401.

Le Roux, D.Y., Pouliot, B., 2008. Analysis of numerically induced oscillations in 2D finite-element shallow-water models Part II: planetary waves. SIAM Journal of Scientific Computing 30, 1971–1991.

Le Roux, D.Y., Rostand, V., Pouliot, B., 2007. Analysis of numerically induced oscillations in 2D finite-element shallow-water models Part I: inertia-gravity waves. SIAM Journal of Scientific Computing 29, 331–360.

Leendertse, J.J, 1967. Aspects of a computational model for long period water wave propagation. Tech Report RM-5294-PR, Santa Monica, Rand Memorandum.

Löhner, R., Oñate, E., 1998. An advancing front point generation technique. Communications Numerical Methods in Engineering 14, 1097–1108.

McCalpin, J.D., 1988. A quantitative analysis of the dissipation inherent in semi-Lagrangian advection. Monthly Weather Review 116, 2330–2336.

Miglio, E., Quateroni, A., Saleri, F., 1999. Finite element approximation of quasi-3D shallow water equations. Computer Methods in Applied Mechanics and Engineering 174, 355–369.

Pain, C.C., Piggott, M.D., Goddard, A.J.H., Fang, F., Gorman, G.J., Marshall, D.P., Eaton, M.D., Power, P.W., de Olivera, C.R.E., 2005. Three-dimensional unstructured mesh ocean modelling. Ocean Modelling 10, 5–33.

Perot, B., 2000. Conservation properties of unstructured staggered mesh schemes. Journal of Computational Physics 159, 58–89.

Pinder, G.F., Gray, W.G., 1977. Finite Elements in Surface and Subsurface Hydrology. Academic Press.

Raviart, P.A., Thomas, J.M., 1977. A mixed Finite Element Method for 2nd Order Elliptic Problems. Mathematical Aspects of the Finite Element Method, Lecture Notes in Math. Springer, Berlin.

Staniforth, A., Côté, J., 1991. Semi-Lagrangian integration schemes for atmospheric models - a review. Monthly Weather Review 119, 2206–2223.

Stelling, G.S., Duinmeijer, S.P.A., 2003. A staggered conservative scheme for every Froude number in rapidly varied shallow water flows. International Journal for Numerical Methods in Fluids 43, 1329–1354.

Strang, G., 1988. Linear Algebra and its Applications. Harcourt Brace Jovanovich College Publishers.

Toro, E.F., 1997. Riemann Solvers and Numerical Methods for Fluid Dynamics. Springer-Verlag, New York. 492 pp.

Walters, R.A., 2005. A semi-implicit finite element model for non-hydrostatic (dispersive) surface waves. International Journal for Numerical Methods in Fluids 49, 721–737.

Walters, R.A., Carey, G.F., 1983. Analysis of spurious oscillation modes for the shallow water and Navier–Stokes equations. Computers and Fluids 11, 51–68.

Walters, R.A., Casulli, V., 1998. A robust, finite element model for hydrostatic surface water flows. Communications in Numerical Methods in Engineering 14, 931–940.

Walters, R.A., Lane, E.M., Hanert, E., 2009. Useful time-stepping methods for the Coriolis term in a shallow water model, Ocean Modelling 28, 66–74.

Walters, R.A., Lane, E.M., Henry, R.F., 2008. Semi-Lagrangian methods for a finite element coastal ocean model. Ocean Modelling 19, 112–124.

White, L., Deleersnijder, E., Legat, V., 2008. A three-dimensional unstructured mesh finite element shallow-water model, with application to the flows around an island and in a wind-driven, elongated basin. Ocean Modelling 22, 26–47.

Yeh, G.T., 1981. Numerical solutions of Navier–Stokes equations with an integrated compartment method (ICM). International Journal for Numerical Methods in Fluids 1 (3), 207–223.